frontiers | Frontiers in Environmental Science

TYPE Original Research
PUBLISHED 26 May 2023
DOI 10.3389/fenvs.2023.1156475

OPEN ACCESS

EDITED BY
Mohamed Ashour,
National Institute of Oceanography and Fisheries (NIOF), Egypt

REVIEWED BY
Ahmed E. Alprol,
National Institute of Oceanography and Fisheries (NIOF), Egypt
Reda S. Salama,
Delta University for Science and Technology, Egypt

*CORRESPONDENCE
Shahid Iqbal,
shahid.iqbal704@yahoo.com
Ali Bahadur,
hderg7561@gmail.com
Eslam B. Elkaeed,
ikaeed@mcst.edu.sa

RECEIVED 02 February 2023
ACCEPTED 05 April 2023
PUBLISHED 26 May 2023

CITATION
Al-Saeedi SI, Areej A, Qamar MT, Alhujaily A, Iqbal S, Alotaibi MT, Aslam M, Qayyum MA, Bahadur A, Awwad NS, Jazaa Y and Elkaeed EB (2023), Isotherm and kinetic studies for the adsorption of methylene blue onto a novel Mn_3O_4-Bi_2O_3 composite and their antifungal performance.
Front. Environ. Sci. 11:1156475.
doi: 10.3389/fenvs.2023.1156475

Isotherm and kinetic studies for the adsorption of methylene blue onto a novel Mn_3O_4-Bi_2O_3 composite and their antifungal performance

Sameerah I. Al-Saeedi[1], Asfa Areej[2], Muhammad Tariq Qamar[2], Ahmad Alhujaily[3], Shahid Iqbal[4]*, Mohammed T. Alotaibi[5], Muhammad Aslam[6], Muhammad Abdul Qayyum[7], Ali Bahadur[8]*, Nasser S. Awwad[9], Yosef Jazaa[10] and Eslam B. Elkaeed[11]*

[1]Department of Chemistry, College of Science, Princess Nourah bint Abdulrahman University, Riyadh, Saudi Arabia, [2]Department of Chemistry, Forman Christian College (A Chartered University), Lahore, Pakistan, [3]Biology Department, College of Science, Taibah University, Al Madinah Al Munawarah, Saudi Arabia, [4]Department of Chemistry, School of Natural Sciences (SNS), National University of Science and Technology (NUST), Islamabad, Pakistan, [5]Department of Chemistry, Turabah University College, Taif University, Taif, Saudi Arabia, [6]Centre of Excellence in Environmental Studies (CEES), King Abdulaziz University, Jeddah, Saudi Arabia, [7]Department of Chemistry, Division of Science and Technology, University of Education, Lahore, Pakistan, [8]Department of Chemistry, College of Science and Technology, Wenzhou-Kean University, Wenzhou, China, [9]Chemistry Department, Faculty of Science, King Khalid University, Abha, Saudi Arabia, [10]Faculty of Engineering, King Khalid University, Abha, Saudi Arabia, [11]Department of Pharmaceutical Sciences, College of Pharmacy, AlMaarefa University, Riyadh, Saudi Arabia

Metal oxide-based adsorbents are quite in for wastewater treatment because of their selectivity, stable structure and very low solubility in aqueous systems. To explore the adsorption of methylene blue (MB), Mn_3O_4-Bi_2O_3 adsorbents were made using a wet-impregnation technique with various concentrations of Mn_3O_4. The presence of Mn_3O_4 contents on the surface of monoclinic Bi_2O_3 was confirmed through representative scanning electron micrographs. The diffractions pertaining to cubic Mn_3O_4 and monoclinic Bi_2O_3 were noticed in the XRD pattern of 5% Mn_3O_4-Bi_2O_3 which confirm the composite nature of the adsorbent. XPS analysis revealed the existance of Bi 4f, Bi 4d, Bi 4p, Bi4s, and Mn 2p core levels in Mn_3O_4-Bi_2O_3. The adsorption study divulged highest efficiency (~95% and qe = ~1.4 mgg^{-1}) of 5% Mn_3O_4-Bi_2O_3 composite among other contestants in removing 30 ppm MB at 28 ° C, pH 7 and 250 rpm. In addition to the determination of adsorption ability, the effect of preliminary dye concentration (5, 10, 20, and 30 ppm) and contact time (0.5–6 h) on the removal efficiency of prepared adsorbents were also monitored. The adsorption data from the batch experiments were evaluated using the Langmuir, Freundlich, Temkin, and Dubinin-Radushkevich-Kaganer (DRK) adsorption isotherms and pseudo 1st and 2nd-order kinetic models. The fitting of adsorption isotherms and kinetic models revealed the formation of adsorbate's monolayer on the surface of adsorbents through the process of chemisorption. Through FTIR measurement, the MB adsorption onto the effective adsorbent (5% Mn_3O_4-Bi_2O_3) was also confirmed. Moreover, TGA analysis showed ~1.5% weight loss by 5% Mn_3O_4-Bi_2O_3 before MB adsorption whereas ~2.6% weight loss was noticed after dye adsorption onto the adsorbent. The antifungal activity was evaluated against the fungi *A. solani* and *M. fructicola* using the agar well

diffusion technique. The 5% Mn_3O_4-Bi_2O_3 composites have exceptional antifungal characteristics compared to Bi_2O_3 and Mn_3O_4, with zone inhibition values of 58.6 and 53.9 mm, respectively.

KEYWORDS

adsorption, kinetic models, isotherms, Mn3O4-Bi2O3 composite, methylene blue

Introduction

It is well-established that the textile industries around the world are utilizing over 1,000 tons of approximately 10,000 commercially available dyes in a year, wherein 10%–15% of these dyes are being released into waterbodies as effluent [(El-Zahhar and Awwad, 2016; Homaeigohar et al., 2016; Hu and Xu, 2020)]. Textile dyes are complex organic toxic compounds that can cause serious threats to the environment if they are not handled properly [(Ayub et al., 2020; Palansooriya et al., 2020; Rahman et al., 2020)]. Moreover, the long-term presence of these dyes in aqueous systems due to their stable chemical structure reduces oxygen contents in water which disturbs aquatic life and produces carcinogenic and mutagenic compounds which pose toxic effects [(Zaharia et al., 2009; Yagub et al., 2014; Hu et al., 2018; Alshorifi et al., 2022)].

Among textile dyes, methylene blue (MB) is an aromatic, cationic and heterocyclic dye. At room temperature, it is an odourless solid dark green powder that turns dark blue when dissolved in water. Due to its exceptional resistance to the stomach's acidic environment and the body's natural hydrolytic enzymes, it is extremely stable in the human body. The liver fails to metabolize the dye and is filtered out through the kidneys. Continuous human exposure to MB can cause serious health issues such as eyes to burn, irritation in the skin and gastrointestinal tract, nausea, profuse sweating, mental confusion, methemoglobinemia, vomiting and diarrhea [(Laurent et al., 2008; Dada et al., 2016; Li et al., 2018)]. Therefore, it is highly desirable to treat MB-contaminated water and finding an effective method to treat contaminated water without producing secondary waste is the prime concern of the day. In this context, studies are underway in the exploration of cost-effective and facile techniques for the cleaning of polluted water without even leaving trivial traces of dyes.

The removal of dyes and high-risk pollutants from water using flexible techniques such adsorption, membrane separation, photocatalysis, electrosorption, electro-flocculation, and nanofiltration has been practised to reduce environmental concerns over the past few decades [(Bakry et al., 2022)]. Among these removal techniques, Adsorption is found to be the best approach that has greater potential to remove toxic dyes, due to its adaptability, economical affordability, low-energy requirements, and easy maintenance mechanism [(Allen and Koumanova, 2005; Li et al., 2020; Ibrahim et al., 2021)]. This technique is mainly based on the forces between the adsorbate and adsorbent. Moreover, being a key component of adsorption the exploration of adsorbents for the whole elimination of organic contaminants from polluted water is highly desirable because there is a lack of actual progress in wastewater treatment due to the inaccessibility of high-capacity adsorbents.

Metal oxide-based adsorbents, owing to high capacity, selectivity, specific surface energy and affinity, chemically stable structure and low solubility are declared efficient contestants for the adsorption of contaminants such as dyes, phenols, pesticides, etc. [(Faraji et al., 2010; De Jesús Ruíz-Baltazar et al., 2019; Mittal et al., 2020)]. Previously, iron oxides, titanium dioxide, cobalt oxide, zinc oxide, aluminum oxide, magnesium oxide and mixed metal oxides in their pure and modified forms were used for the treatment of dye-containing water [(Krishnan et al., 2022)]. A couple of years ago, Das and Sharma synthesized Gd_2O_3/Bi_2O_3@rGO adsorbent for the elimination of methyl orange dye and optimized the parameters for efficient adsorption of adsorbate. [(Das and Sharma, 2020)]. Recently, Adam *et. al* described an increase in the adsorption efficiency of MgO with the increasing content of Bi_2O_3 for the removal of indigo carmine [(Adam et al., 2022)]. While taking the advantage of metal oxide-based adsorbents, in this study an effort has been made to prepare novel composites of surface altered monoclinic Bi_2O_3 with varying amounts of Mn_3O_4 using wet-impregnation methodology. The synthesized nanocomposites were further utilized to remove 30 ppm MB from the contaminated water. Moreover, different kinetic models and adsorption isotherms were also studied to investigate the phenomenon of adsorption of MB on newly synthesized composites. As this study was not done before while taking into account the removal of MB by Mn_3O_4-Bi_2O_3 composites through the adsorption process, however, effecincy of a few metal oxide-based adsorbents were reported for the adosprion of MB [(Gómez-Pastora et al., 2014; Yang et al., 2014; Li et al., 2019; Naseri and Allahverdi, 2019; Alomar et al., 2021)]. Morover, this study provides a sufficient insight about the synthesis and characterization of novel Mn_3O_4-Bi_2O_3 adsorbent having excellent adsorption efficiency prepared through surface modification technique for the removal of MB dye.

Experimental

Materials

Manganese (II) nitrate tetrahydrate [Mn(NO3)2.4H2O, Sigma-Aldrich, ≥ 97%], Ethanol (C_2H_5OH, Sigma-Aldrich, ≥ 99.8%), Bismuth (III) nitrate pentahydrate [Bi(NO3)3.5H2O, Sigma-Aldrich, ≥ 98%], Acetone [CH_3COCH_3, Sigma-Aldrich], Nitric acid [HNO_3, Sigma-Aldrich, 70%], potassium hydroxide [KOH, Sigma-Aldrich, 99.5%], Distilled water and Triton X-100 [Tx-100, Sigma-Aldrich] were used without further purification for the synthesis of Bi_2O_3-based adsorbents. These synthesized composites were used to remove MB [$C_{16}H_{18}ClN_3S$, Sigma-Aldrich, ≥ 95%], the target pollutant, from the contaminated water.

Surfactant-assisted synthesis of α-Bi_2O_3 and Mn_3O_4 adsorbents

α-Bi_2O_3 and Mn_3O_4 were synthesized as per the reported method [(Hameed et al., 2015; Qamar et al., 2017a)]. In a typical synthesis of α-Bi_2O_3, 25 g Bi $(NO_3).5H_2O$ was dissolved

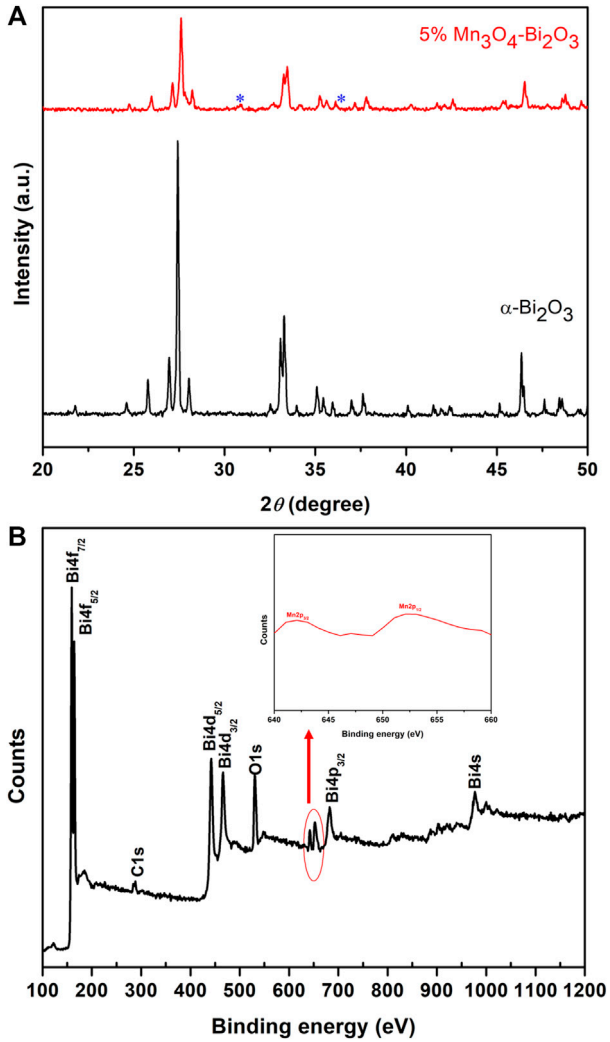

FIGURE 1
(A) The comparison of XRD patterns of Bi_2O_3 and 5% Mn_3O_4-Bi_2O_3 in 2θ range of 20° –50° and **(B)** the wide angle XPS survey scan of 5% Mn_3O_4-Bi_2O_3 composite.

in a solvent containing 85 mL distilled water and 15 mL nitric acid at 50 ° C with continuous stirring till the formation of a clear solution. 3 mL TX-100 was added into the solution while continuing the stirring for 2 h. The Bi^{3+} solution was hydrolyzed with slow addition of KOH till the formation of yellow (gel) precipitates at pH 8 under vigorous stirring. The precipitate was filtered through Whatman filter paper and repeatedly rinsed with distilled water, ethanol, and acetone to achieve a pH neutral precipitate. The resulting precipitate was dried for 8 h at 100°C in a hot air oven. The precipitate was also pulverised and calcined at 500°C for 4 h in a Vulcan D-550 muffle furnace.

Mn_3O_4 was synthesized by dissolving 10 g Manganese (II) nitrate tetrahydrate in distilled water. After the complete dissolution of the precursor in distilled water, 3 mL surfactant TX -100 was added. The surfactant-containing solution was hydrolyzed with the slow addition of 0.5 M KOH till pH 8 with stirring at 50 ° C and the solution immediately turned into dark brown precipitate. The mixture was further heated and stirred for 20 min to ensure the complete formation of precipitate. The precipitate was then filtered using Whatman filter paper, and the surfactant and alkali content were removed by repeatedly washing the filtrate in distilled water, ethanol, and acetone. The precipitate was dried for 8 h in an oven at 100°C. The brown precipitate was powdered later, and it was then calcined for 4 hours at 500°C in a Vulcan D-550 muffle furnace.

Synthesis of Mn_3O_4-Bi_2O_3 adsorbents using wet-impregnation

Mn $(NO_3)_2.4H_2O$ was used to prepare 1, 3, 5, and 10 wt% composites of Mn_3O_4-Bi_2O_3 using the wet-impregnation method by varying the amount of Mn concerning the fixed weight of Bi_2O_3. In a typical synthesis of 1% Mn_3O_4-Bi_2O_3 composite, 0.23 g Mn $(NO_3)_2.4H_2O$ was disbanded in 50 mL distilled water at 50 ° C with continuous stirring till the formation of a clear solution

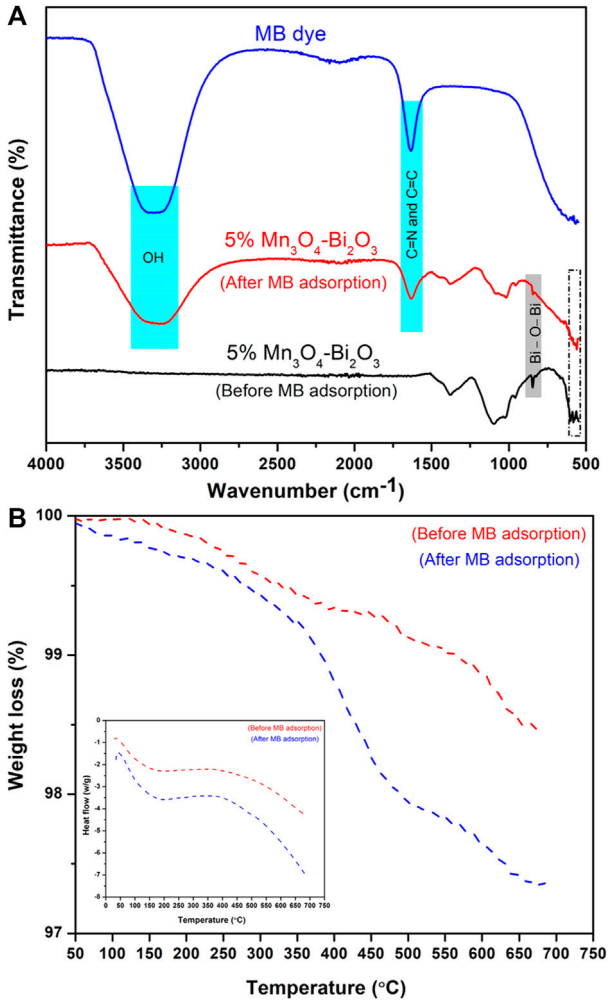

FIGURE 2
(A) The comparison of FTIR spectra of MB and 5% Mn_3O_4-Bi_2O_3 adsorbent and **(B)** the TGA/DSC curves of 5% Mn_3O_4-Bi_2O_3 composite.

(Scheme 1). After the complete dissolution of the Manganese precursor, 5 g pre-synthesized Bi_2O_3 was inserted and the blend was heated at 150 ☐C till complete dryness to obtain 1% Mn_3O_4-Bi_2O_3 composite. The dried composite was scratched from the beaker, ground and subjected to calcination at 500°C for 4 h in a furnace. Finally, the composite was again ground and saved in the labeled airtight glass vials for further use. Literature reveals that composites of metal oxides can be prepared successfully through wet-impregnation methodology [(Qamar et al., 2017b; Alhogbi et al., 2020)]. Therefore, the same wet-impregnation method as stated above was used for the preparation of 3, 5, and 10 wt% Mn_3O_4/Bi_2O_3 composites while taking 0.68 g, 1.14 g and 2.28 g of Mn $(NO_3)_2.4H_2O$, respectively.

Characterization of the synthesized material

By using an X'pert X-ray powder diffractometer (Philips PW1398) with a Cu K radiation source at 40 mA electric current and 40 kV operating voltage, XRD patterns were acquired from 10o to 80o with 0.01o step size. The PHI 5000 Versaprobe II X-ray photoelectron spectrometer captured the XPS survey scan of the 5 percent Mn_3O_4-Bi_2O_3 sample in the binding energy range of 0–1,350.08 eV. The morphology of the synthesized adsorbents was evaluated by scanning electron microscope (TESCAN LYRA3). Thermal stability of 5% Mn_3O_4-Bi_2O_3 before and after adsorption was inspected using TA instruments SDT Q600 TGA/DSC analyzer in N_2 environment from 0°C to 700°C at 20°C/min rate. FTIR spectra of MB and 5% Mn_3O_4-Bi_2O_3 were recorded before and after adsorption ranging from 550 to 4,000 cm^{-1} using Bruker Alpha II FTIR spectrometer.

Adsorption study

Synthetic wastewater composed of MB was used as an adsorbate and its four various contents, i.e., 5, 10, 20, and 30 ppm were prepared in distilled water by dissolving 5, 10, 20, and 30 mg MB, respectively. In the first phase, 6 different conical flasks containing 50 mL 30 ppm MB were taken and then 1 g of each adsorbent, i.e., Bi_2O_3, Mn_3O_4, 1, 3, 5, and 10 wt% Mn_3O_4-Bi_2O_3

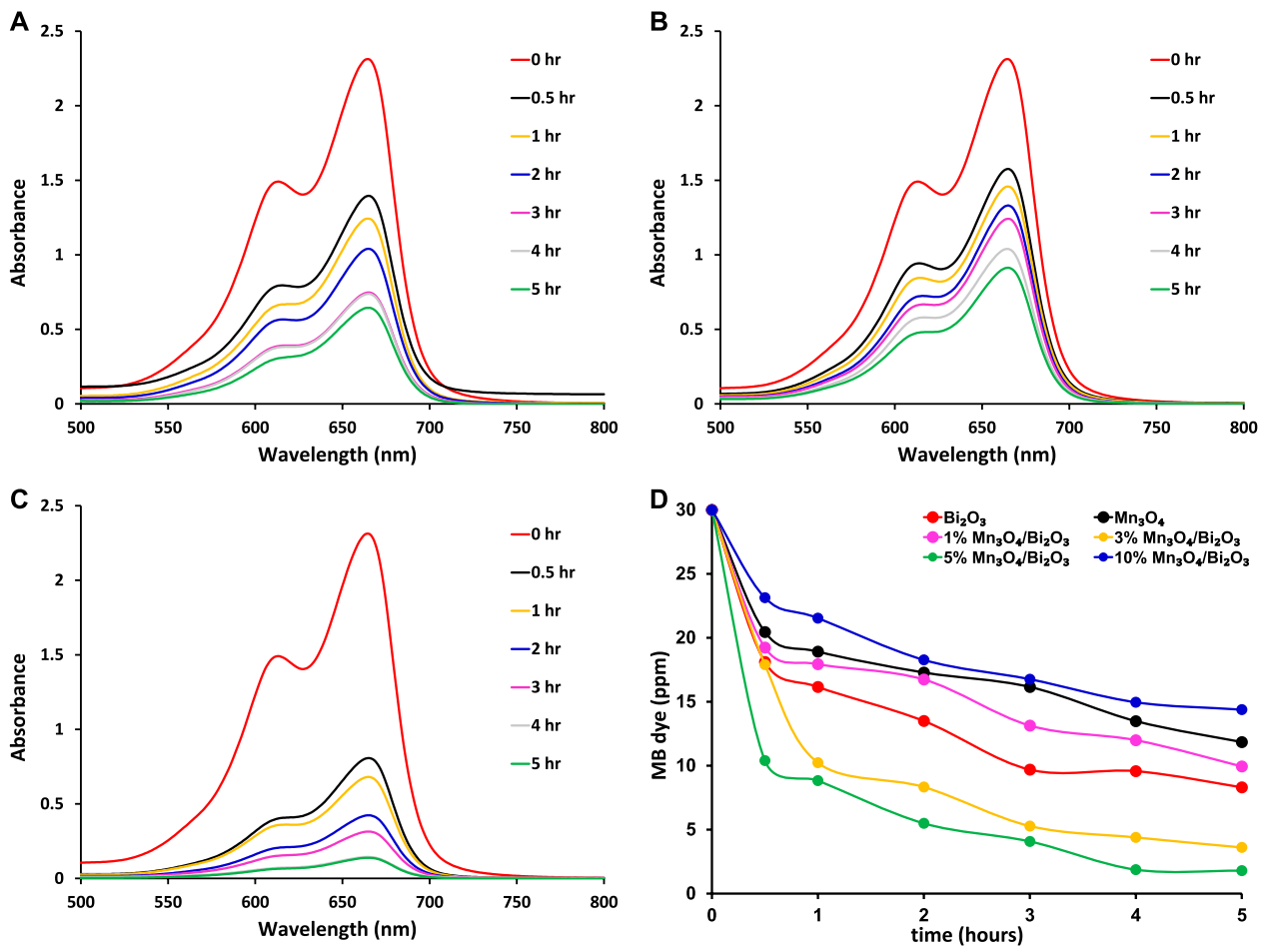

FIGURE 3
The comparison of UV-Vis. absorption of unadsorbed MB at 665 nm after adsorption on prepared **(A)** Bi_2O_3 **(B)** Mn_3O_4 and **(C)** 5% Mn_3O_4-Bi_2O_3 adsorbents at 28 ° C, 7 pH and 250 rpm whereas **(D)** represents the comparison of decrease in concentration of MB after adsorption on synthesized adsorbents.

TABLE 1 Removal of MB by few reported metal oxide-based adsorbents.

Adsorbent	Removal of MB (%)	Reference
Fe_3O_4	50-53	24
GO-Fe_3O_4@P4VP	99	25
TiO_2	90	26
Bi_2O_3-SrO-FeO@SiO_2	94	27
$MnFe_2O_4$	98	28
Magnetic cellulose/GO	97	43
5% Mn_3O_4-Bi_2O_3	95	this study

was added in the flasks, respectively. The flask having a heterogeneous mixture of adsorbate and adsorbent were shaken in an orbital mechanical shaker at 250 rpm, 28 ☐C, 7 pH for 5 h. The adsorption of MB on each adsorbent was monitored by collecting samples from each flask after 30, 60, 120, 180, 240, and 300 min (contact time) shaking time. The filtered samples were measured for percent adsorption and adsorption capacity (q_t) using the following equations in a UV-Visible spectrophotometer after being filtered with a syringe filter [(Mahmoud and Mahmoud, 2021; Kasbaji et al., 2022)]:

$$\%\, adsorption = \frac{(C_\circ - C_t)}{C_\circ} \times 100 \quad (1)$$

$$q_t = \frac{(C_\circ - C_t)V}{W} \quad (2)$$

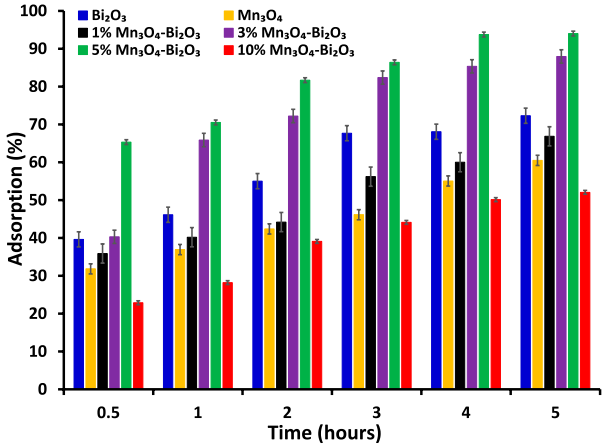

FIGURE 4
The comparison of percentage adsorption of 30 ppm MB on different adsorbents at 28 ° C, 7 pH and 250 rpm.

Where C_o is the initial concentration of the adsorbate; C_t is the concentration of the adsorbate at any time (t); V is the volume of adsorbate in (l) and W is the amount of adsorbent in grams (g). The MB concentration was calculated using UV-Visible spectrophotometer at 665 nm (λ_{max}). In the second phase, a similar adsorption procedure as stated above was followed to study the adsorption of 5, 10, 20 and 30 ppm MB on 5% Mn_3O_4-Bi_2O_3 adsorbent for 480 min shaking time. After an hour, the samples were collected and put through a syringe filter. Using Eqs 1, 2, the obtained samples were then exposed to a UV-Visible spectrophotometer for the purpose of determining the percent adsorption and adsorption capacity.

Study of kinetic models and adsorption isotherms

The adsorption process of MB on Bi_2O_3- based adsorbents at 28 ° C, 7 pH and 250 rpm was explored by applying pseudo 1st and 2nd-order kinetic models and four adsorption isotherms, i.e., Freundlich, Langmuir, Dubinin-Raduskavich-Kaganer (DRK), and Temkin [(Mahmoud and Mahmoud, 2021; Kasbaji et al., 2022)].

Recycling of 5% Mn_3O_4-Bi_2O_3 adsorbent

Initially, the regeneration study was performed in a 250 mL beaker using 90% ethanol as per reported method (Li et al., 2020). Secondly, the conical flask containing suspension composed of 1.0 g regenerated 5% Mn_3O_4-Bi_2O_3 adsorbent and 50 mL 30 ppm MB adsorbate was placed in a n orbital mechanical shaker at 28 ° C, 7 pH and 250 rpm for 4 hs. In order to determine the percent adsorption using Eq. 1, the sample was collected, filtered with a syringe filter, and then tested in a UV-Visible spectrophotometer. This experiment was repeated three times for regeneration of adsorbent and then its reuse for the adsorption of 30 ppm MB.

Results and discussion

Characterization of the synthesized material

XRD patterns of the designed Bi_2O_3 and 5% Mn_3O_4-Bi_2O_3 adsorbents are presented in Figure 1A. A moboclinic phase of α-Bi_2O_3 with lattice parameters (a = 5.8486 Å, b = 8.1661 Å, c = 7.5097 Å an d α = γ = 90°, β = 113°) proven by coordinating diffractions patterns with ICDD# 01-071-2,274. A noticeable decrease in the intensity, peak broadening and a minor shift in the positions of diffractions pertaining to Bi_2O_3 were observed with the addition of Mn_3O_4. The literature and the observed reflections caused by Bi_2O_3 and Mn_3O_4 are in good accord [(Li et al., 2014; Sood et al., 2015; Astuti et al., 2016)]. Moreover, the presence of (220) and (311) planes of cubic Mn_3O_4 (*) which are clearly dominated by the Bi_2O_3 diffractions is also noticed in Figure 1A that further confirms the composite nature of the synthesized adsorbent. The crystallite size of Bi_2O_3 before and after composite formation by selecting the most intense peak at (2θ) 27.48° and 27. 61°, respectively was estimated using Debye–Scherrer equation. Where a significant decrease in crystallite size (~40.43 nm) was noticed after composite formation as compared to ~80.83 nm crystallite size of Bi_2O_3. XPS survey scan of 5% Mn_3O_4-Bi_2O_3 is provided in Figure 1B, wherein the peaks related to splitted and core levels of componets of the composite, i.e., Bi4f, Bi4d, Bi4p, Mn2p, O1s are observable. The presence of all peaks at binding energy values are in agreement with literature values [(Li et al., 2014; Hameed et al., 2015; Sood et al., 2015; Astuti et al., 2016; Qamar et al., 2017a; Qamar et al., 2017b; Alhogbi et al., 2020; Mahmoud and Mahmoud, 2021; Kasbaji et al., 2022)].

The FTIR spectra of 5% Mn_3O_4-Bi_2O_3 composite (before and after adsorption) and MB dye are presented in Figure 2A, where the bands due to Bi-O-Bi and Mn-O vibrations at 846 cm^{-1} and 574 cm^{-1} are observable in 5% Mn_3O_4-Bi_2O_3. The appearance of these bands is in close accordance with the literature, which further confirms the composite nature of the adsorbent [(Zulkifli et al., 2018; Khan and Wahab, 2022)]. A borad band at 3,299 cm^{-1} is attributed

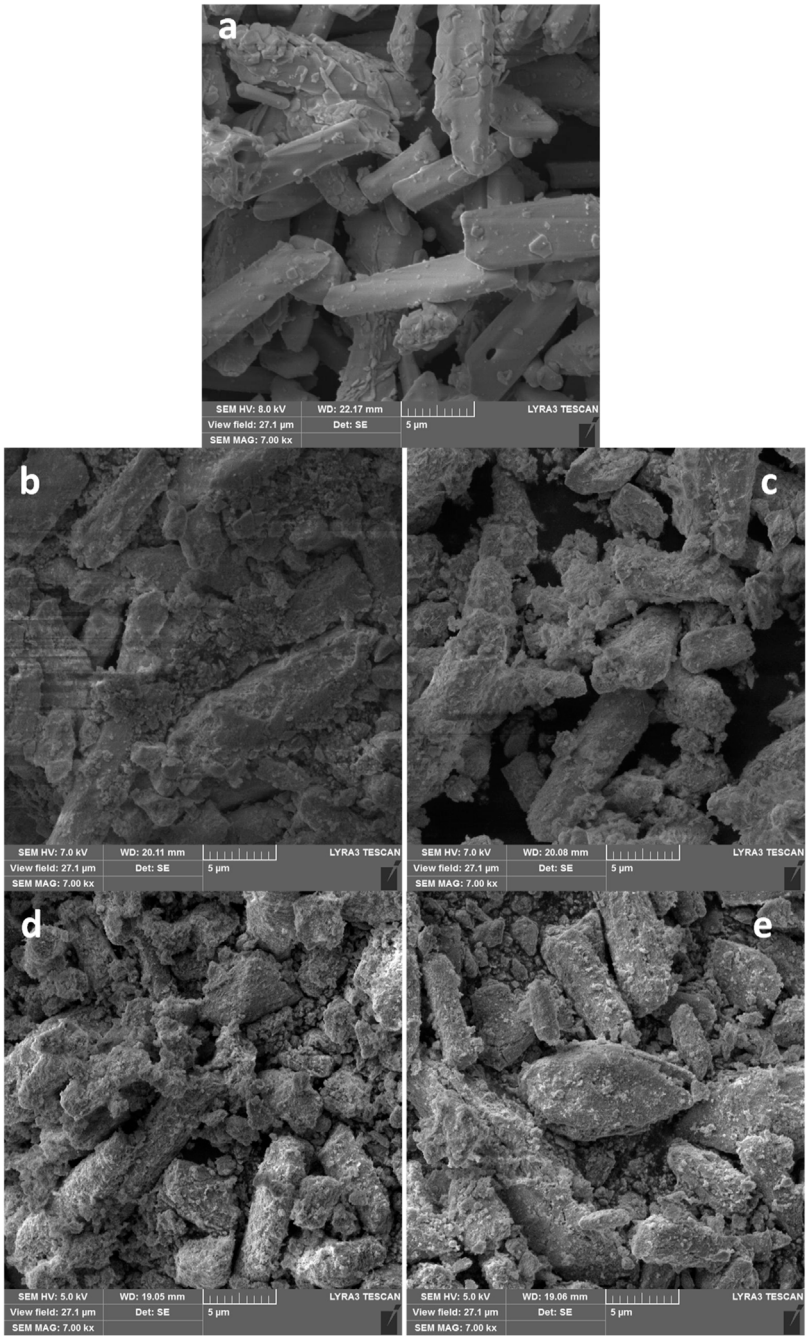

FIGURE 5
The scanning electron micrographs of **(A)** Bi_2O_3 **(B)** 1 wt% **(C)** 3 wt% **(D)** 5 wt% and **(E)** 10 wt% Mn_3O_4-Bi_2O_3 adsorbents at 7.00 kx magnifications.

to OH groups in aqueous solution of MB whereas a peak appeared at 1,636 cm^{-1} is mainly due to vibrations of C=N and C=C groups in aromatic rings of MB [(Raiyaan et al., 2021; Birniwa et al., 2022)].

FTIR spectrum of 5% Mn_3O_4-Bi_2O_3 composite shows a decrease in Bi-O-Bi and Mn-O bands after the adsorption of MB. In addition, the peaks due to OH and aromatic rings related to MB solution with minor shift are also observed in FTIR spectrum of adsorbent after adsorption. The reduction in peak intensity and shifts in band positions as shown in Figure 2A further authorise the binding of MB dye with adsorbent. The thermal stability of the 5% Mn_3O_4-Bi_2O_3 composite was investigated through TGA/DSC as shown in Figure 2B, where the composite experienced a weight loss of about 1.5%; however, after the MB dye was adsorbed, this loss increased to a maximum of 2.6%. The main cause of this comparatively larger weight loss is the desorption of water and MB molecules from the adsorbent's surface (Naeem et al., 2016). Moreover, the higher stability and lower content degradation rate of 5% Mn_3O_4-Bi_2O_3 composite was noticed before adsorption in comparison to after MB adsorption as presented in DSC curves given in inset of Figure 2B.

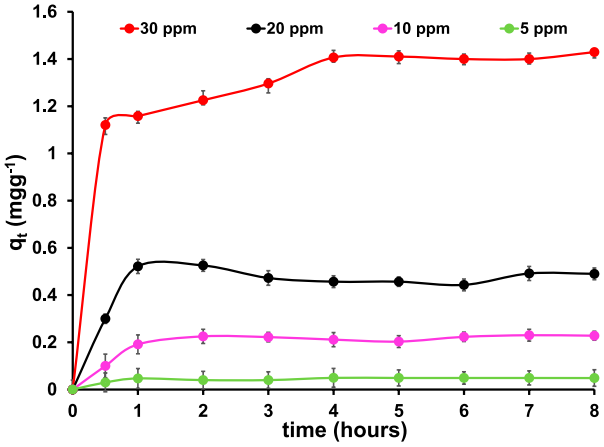

FIGURE 6
Effect of preliminary MB concentration on adsorption capacity of 5, 10, 20 and 30 ppm MB dye at 28 ° C, 7 pH and 250 rpm on 5% Mn_3O_4/Bi_2O_3 adsorbent.

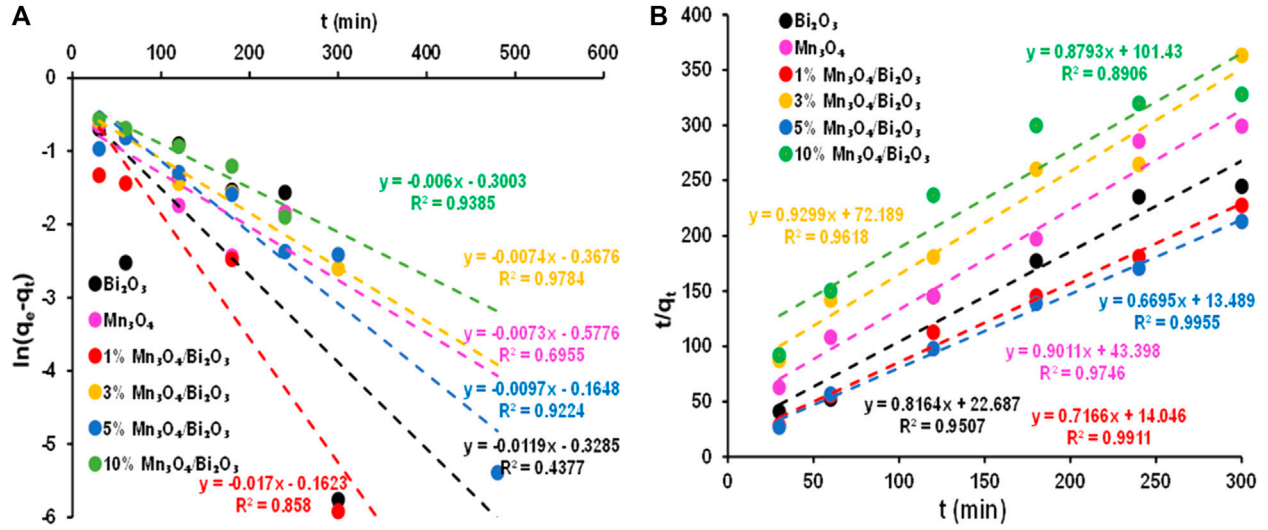

FIGURE 7
Linearized plots of **(A)** pseudo 1st order and **(B)** pseudo 2nd order for the adsorption of 30 ppm MB at 28 ° C, 7 pH and 250 rpm on synthesized adsorbents.

Dye adsorption onto synthesized adsorbents

Using a UV-visible spectrophotometer, the adsorption of 30 ppm MB on the unaltered and modified Bi_2O_3 was observed. The spectra captured after various shaking periods are shown in Figure 3. The comparison of MB removal shows that the maximum adsorption of the pollutant was noticed by 5% Mn_3O_4-Bi_2O_3 composite among all synthesized adsorbents whereas its comparion with few previously studied metal oxide-based adsorbents is given in Table 1. Moreover, the continuous decrease in MB concentration with increasing contact time for all adsorbents can be seen in Figure 3d. The efficient adsorbent 5% Mn_3O_4-Bi_2O_3 was able to remove ~95% MB (qe = ~ 1.4 mgg^{-1}) in 4 h at 28 ° C, 7 pH and 250 rpm, whereas ~65% and ~55% MB was removed by unmodified Bi_2O_3 and Mn_3O_4 in same contact time, respectively as shown in Figure 4. This higher dye removal by 5% Mn_3O_4-Bi_2O_3 composite may recognized to the existence of more probable adsorption sites as compared to other prepared adsorbents.

The possible greater adsorption of MB on 5% Mn_3O_4-Bi_2O_3 as compared to Bi_2O_3 was attributed to the increase in capturing sites than pure Bi_2O_3. Whereas, the lower dye removal by 10% Mn_3O_4-Bi_2O_3 may be due to the greater content of Mn_3O_4 which showed lower adsorption of MB when it was used alone. Therefore, a proper balance between the quantities of both components in a composite is an important factor to consider while synthesing adsorbents for dye removal from polluted water. Due to the existence of more

TABLE 2 Kinetic variables for the 30 ppm MB adsorption on the created adsorbents.

Adsorbents	Pseudo 1st order			Pseudo 2nd order			q_e (exp.) (mg/g)
	k_1 (min^{-1})	q_e (mg/g)	R^2	k_2 (g/mg min^{-1})	q_e (mg/g)	R^2	
Bi_2O_3	0.0119	0.72	0.4377	0.0294	1.2249	0.9507	1.0153
Mn_3O_4	0.0073	0.5612	0.6955	0.0187	1.1097	0.9746	1.0030
1% Mn_3O_4-Bi_2O_3	0.0170	0.8502	0.858	0.0366	1.3955	0.9911	1.3255
3% Mn_3O_4-Bi_2O_3	0.0074	0.6924	0.9784	0.0121	1.0754	0.9618	0.9312
5% Mn_3O_4-Bi_2O_3	0.0097	0.8481	0.9224	0.0330	1.4936	0.9955	1.4105
10% Mn_3O_4-Bi_2O_3	0.0060	0.7406	0.9385	0.0076	1.1373	0.8906	0.9147

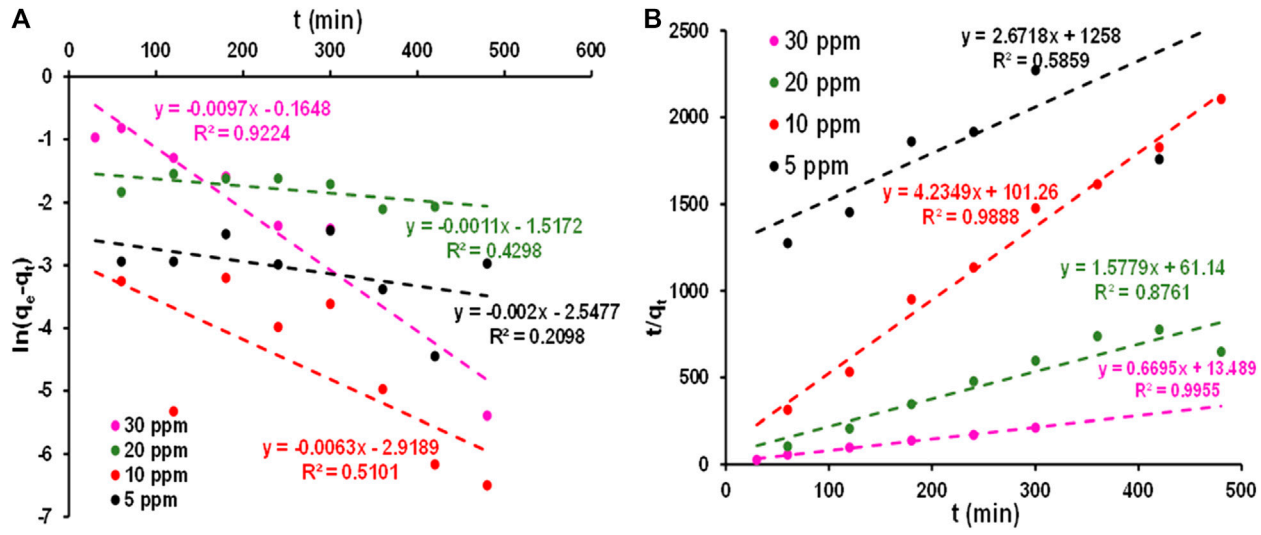

FIGURE 8
Linearized plots of **(A)** pseudo 1st order and **(B)** pseudo 2nd order for the adsorption of 5, 10, 20 and 30 ppm MB at 28 ° C, 7 pH and 250 rpm on 5% Mn_3O_4-Bi_2O_3.

TABLE 3 Kinetic factors for the 5, 10, 20, and 30 ppm MB adsorption on the 5% Mn_3O_4-Bi_2O_3 surface.

Dye methylene blue concentration (ppm)	Pseudo 1st order			Pseudo 2nd order			q_e (exp.)
	k_1 (min^{-1})	q_e (mg/g)	(mg/g)	k_2 (g/mg min^{-1})	q_e (mg/g)	R^2	
5	0.0020	0.0783	0.2098	0.0057	0.3743	0.5859	0.0486
10	0.0063	0.0541	0.5101	0.1772	0.2362	0.9888	0.2279
20	0.0011	0.2193	0.4298	0.0408	0.6337	0.8761	0.0491
30	0.0097	0.8481	0.9224	0.0330	1.4936	0.9955	1.4105

captacuring sites on the surface of the composite adsorbent than on the surface of unmodified Bi_2O_3, as seen in Figure 5D, the enhanced removal effectiveness of 5% Mn_3O_4-Bi_2O_3 was further strengthened. Additionally, the surface of Bi_2O_3 in composites was found to have smaller Mn_3O_4 aggregates; however, the unmodified surface of monoclinic Bi_2O_3 without aggregates is clearly visible in the scanning electron micrographs shown in Figure 5.

Effect of initial concentration of adsorbate and contact time

The effect of different concentrations of MB on the adsorption efficiency of 5% Mn_3O_4-Bi_2O_3 was investigated with four different concentrations of MB dye such as 5, 10, 20, and 30 ppm at different contact times. Figure 6 shows the graphs that show how varied initial

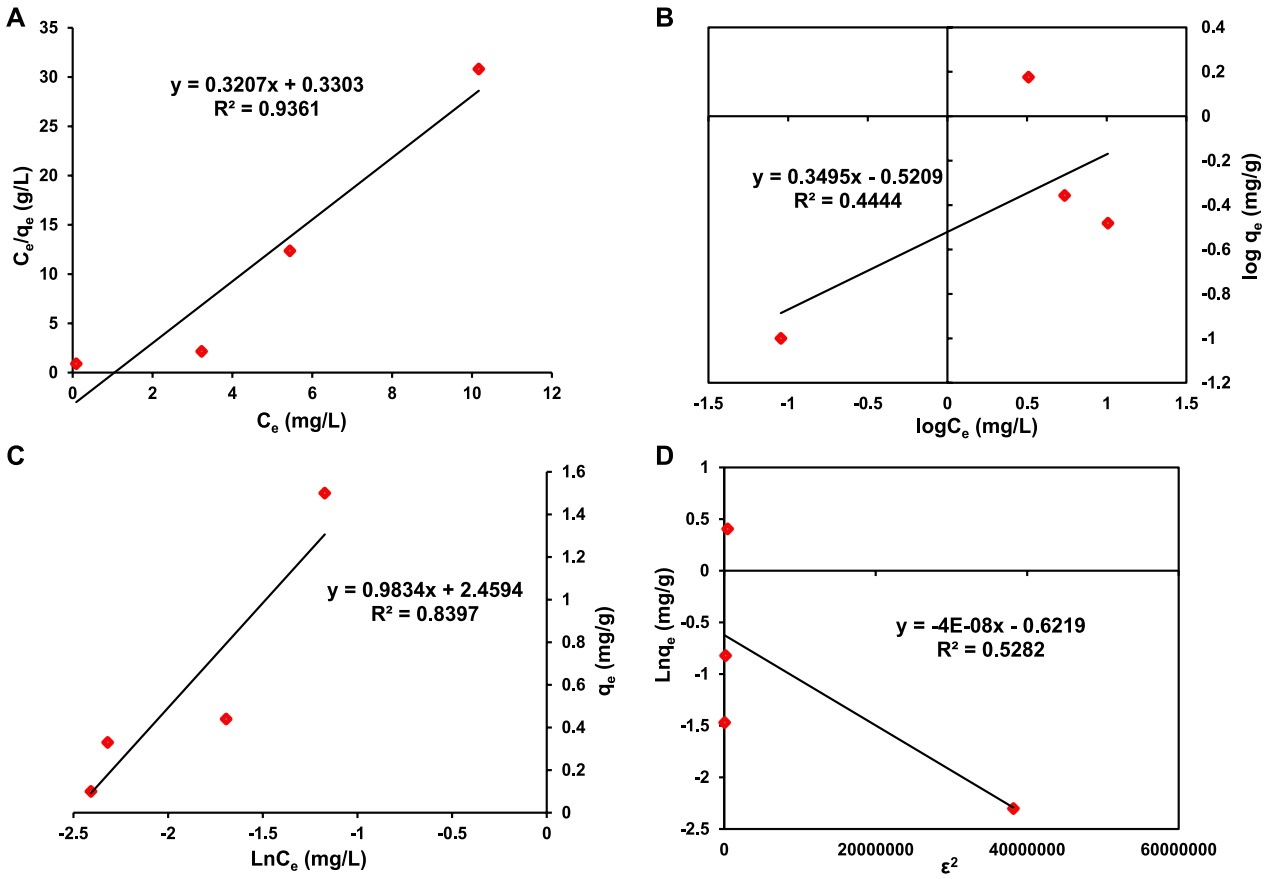

FIGURE 9
Adsorption isotherms **(A)** Langmuir **(B)** Freundlich **(C)** Temkin **(D)** Dubinin-Raduskavich-Kaganer (DRK).

MB concentrations affect adsorption capacity. As the initial concentration of MB rises, the contact time has a substantial impact on the adsorption mechanism because there are more active sites accessible. However, after some time, the equilibrium is reached, and the adsorption becomes constant as illustrated in Figure 6. Moreover, a similar trend was also noticed in few previously reported adsoprtion studies [(Al-Ghouti et al., 2009; Shi et al., 2014; Basu et al., 2018)]. It is observed that in initial 30 min, the fastest adsorption occurs at all concentrations. The plot (q_t vs. t) clearly shows that a condition of dynamic equilibrium is reached after a certain contact time and the value of q_t becomes constant. This equilibrium is a state where the rate of adsorption and desorption becomes equal [(Tan et al., 2008; Ishak and Kumar, 2022)]. It is also evident from the Figure 6 that the process of MB adsorption does not substantially change after equilibrium time. Moreover, The curves show that the equilibrium condition of the 30 ppm MB dye took 4 h to reach, whereas the equilibrium states of the other concentrations (5, 10, and 20 ppm) were almost reached after 2 h of contact time.

As the process of adsorption involves, firstly the mass transfer of dye molecules to the adsorbent's surface, i.e., external diffusion. Secondly, the dye molecules starts attaching and forming a thin film onto the surface of adsorbent, i.e., actual adsorpton and finally the diffusion of adsorbed dye molecules in the pores of adsorbent, i.e., interior diffusion [(Abou-Gamra and Ahmed, 2015)]. It is observed that at a lower concentration of MB, adsorption equilibrium is achieved earlier than higher MB concentration as shown in Figure 4. Which suggests that MB dye removal process mainly follows actual adsorption phenomenon instead of internal and external diffusion phenomena at lower MB concentration whereas the removal of 30 ppm MB is found to be controlled by both actual adsorption and internal diffusion processes [(Abou-Gamra and Ahmed, 2015; Amadi et al., 2017)].

Kinetic models

The adsorption rate of 30 ppm MB on all synthesized adsorbents is evaluated through pseudo 1st and pseudo 2nd-order kinetic models. The models were used to predict the nature of adsorption and determination of adsorption rate constants. Moreover, R^2 values were used to deveolp a correlation between experimental data and kinetic models. The kinetics of adsorption are assumed to be inversely related to dye concentration and directly proportional to the availability of sites on the adsorbent's surface in the pseudo-first order kinetic model. The rate constant (k_1) was determined using following pseudo 1st-order kinetic model equation [(Kasbaji et al., 2022)]:

$$\ln(q_e - q_t) = ln\, q_e - k_1 t \quad (3)$$

TABLE 4 Parameters of adsorption Isotherms.

Dye	Langmuir isotherm				Freundlich isotherm			
Methylene Blue	q_{max} (mg/g)	k_L (L/mg)	R^2		1/n	n (mg/g)	K_f (mg/g)	R^2
	3.12	0.97	0.93		0.35	2.86	0.30	0.44
	Temkin Isotherm				Dubinin-Radushkevich Isotherm			
	A_T (L/g)	b_T (J/mol)	B (L/g)	R^2	q_d (mg/g)	K_{DRK} (mol^2/kJ^2)	E (kJ/mol)	R^2
	12.21	2,565	0.98	0.83	0.54	4×10^{-8}	3.53	0.52

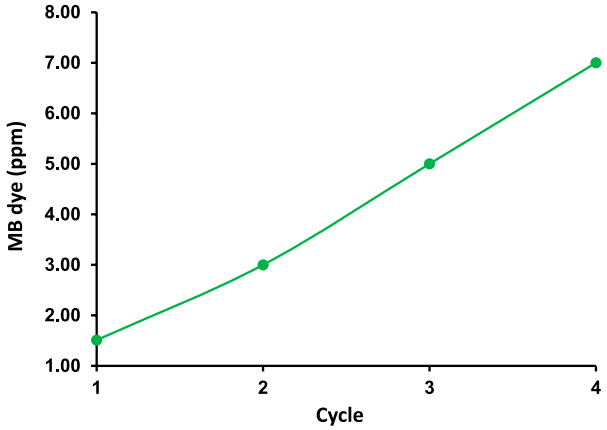

FIGURE 10
Reusability of 5% Mn_3O_4-Bi_2O_3 adsorbent at 28 ° C, 7 pH and 250 rpm in four cycles.

where k_1 (min^{-1}) is the rate constant and q_e and q_t are the amounts of MB dye adsorbed (mg/g) at equilibrium and a time t (minutes), respectively. Additionally, as shown in Figure 7A, the values of k_1 and q_e are determined from the slope and intercept of the plot, respectively.

Contrary to pseudo 1st-order, pseudo 2nd-order presumes that the rate constant is directly proportional to available active sites of adsorbents. This kinetic model is applied to examine the chemisorption kinetics of dye and adsorbent. The linear equation of Pseudo 2nd-order is given below [**34**]:

$$\frac{t}{q_t} = \frac{1}{k_2 q_e^2} + \frac{t}{q_e} \quad (4)$$

All the parameters are well described above. The plot of t/q_t against t shown in Figure 7B can be used to determine the value of constant k_2 (g/mg min).

Pseudo 1st-order and 2nd-order plots for Bi_2O_3, Mn_3O_4, 1% Mn_3O_4-Bi_2O_3, 3% Mn_3O_4-Bi_2O_3, 5% Mn_3O_4-Bi_2O_3 and 10% Mn_3O_4-Bi_2O_3 are shown in Figure 7. These graphs and the kinetic parameters in Table 2 make it clear that practically all adsorbents have greater linear regression coefficients in pseudo 2nd-order kinetic models than in 1st-order kinetic models. Accordingly, pseudo first order provides a poor description of the kinetics of all the adsorbents stated above, while pseudo second order provides the best fit for the kinetics of the adsorption of 30 ppm MB on all the adsorbents. This kinetic study suggests that the adsorption of 30 ppm MB on synthesized adsorbents follows chemical adsorption mechanism wherin the adsorbent surface is playing a rate-limiting role [(Ramutshatsha-Makhwedzha et al., 2022; Nayl et al., 2023)].

The adsorption of 5, 10, 20, and 30 ppm MB onto a 5 percent Mn_3O_4-Bi_2O_3 adsorbent was also examined using pseudo 1st order and pseudo 2nd order kinetics, and the corresponding plots and kinetic parameters are shown in Figure 8 and Table 3, respectively. The favorability of the kinetic models was decided based on R^2 values and adsorption data was found to agree with the pseudo 2nd order model. Which was adequate proof that MB was chemisorption on a 5 percent Mn_3O_4-Bi_2O_3 composite, which revealed the necessity of electron sharing or exchange between MB and the surface of the adsorbent to complete the adsorption process.[(Li et al., 2015; Ahmadi et al., 2020)]. Additionally, it is probable that a decrease in adsoptive sites at the surface of the adsorbent is to blame for the observed decrease in k_2 with an increase in dye concentration. [(Rápó and Tonk, 2021; Tejada-Tovar et al., 2021; Al-Gorair et al., 2022)]

Adsorption isotherms

The adsorption isotherms evaluate the relationship between unadsorbed and adsorbed adsorbate at an equilibrium state. According to the literature, it is vital for adsorption related studies to analyse the data after fitting it into different adsorption isotherms. Additionally, the interpretation of isotherms is a critical procedure but necessary to design an effective adsorption process. The results obtained from isotherms are used to optimize the

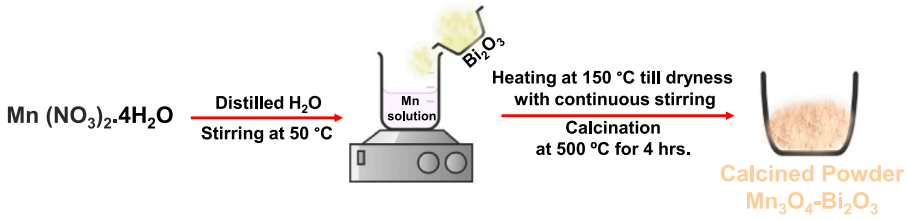

SCHEME 1
Schematic diagram for the synthesis of Mn_3O_4-Bi_2O_3 composite using wet-impregnation method.

TABLE 5 Zone of inhibition for the antifungal activity of Bi2O3, Mn3O4, and 5% Mn3O4-Bi2O3 using the Agar Well diffusion method.

Bacterial strains	Samples	Blank	Zone of Inhibition (mm)
Antifungal Potential			
A. solani	Bi_2O_3	0	39.7
	Mn_3O_4	0	43.1
	5% Mn_3O_4-Bi_2O_3	0	58.6
M. fructicola	Bi_2O_3	0	37.8
	Mn_3O_4	0	39.8
	5% Mn_3O_4-Bi_2O_3	0	53.9

adsorbent properties and further help to understand the adsorption mechanism because each isotherm model evaluates certain physical and chemical properties needed for the adsorption process [(Das and Sharma, 2020; Adam et al., 2022)]. In order to get a detail insight about the adsorption of methylene blue onto 5% Mn_3O_4-Bi_2O_3 the following adsorption isotherms have been applied in this study. Moreover, the applicability of these isotherms is evaluated by comparing respective correlation coefficient (R^2) values.

According to the Langmuir adsorption isotherm, the development of a homogenous monolayer of dye molecules on the adsorbent surface triggers the adsorption of the adsorbate. Additionally, it is claimed that only certain active sites underwent adsorption and that no interactions between adsorbed molecules and phase transitions exist. Additionally, the Langmuir adsorption isotherm is described by the following equation [**33, 34**]:

$$\frac{C_e}{q_e} = \frac{1}{K_L q_{max}} + \frac{C_e}{q_{max}} \quad (5)$$

where C_e denotes the adsorbate concentration at equilibrium (MB) and q_e is the amount of dye adsorbed in (mg/g) at equilibrium. While K_L (l/mg) is the Langmuir constant, which is connected to the adsorption energy, and qmax (mg/g) is the maximum adsorption capacity. The C_e/q_e and C_e representative graph is presented in Figure 9A, and Table 3 contains the evaluated values. The crucial component of the Langmuir isotherm, generally referred to as the separation factor, is another dimensionless quantity, R_L. The following equation is used to calculate this parameter [(Kasbaji et al., 2022)].

$$R_L = \frac{1}{1 + K_L C_0} \quad (6)$$

The R_L value indicates whether it is linear (R_L = 1), irreversible (R_L = 0), favorable (0< R_L <1) or unfavorable (R_L >1). R_L value investigated for this study is 0.0004 which depicts that the adsorption of MB dye on 5% Mn_3O_4/Bi_2O_3 is favorable.

The heterogeneous surface of the adsorbent is studied via the Freundlich adsorption isotherm for both monolayer and multilayer adsorption. It also explains why the molecules that have been adsorbed repel one another. Additionally, it assesses the active spots' exponential distribution and potential energies. The following equation presents the Freundlich isotherm's linear representation [(Kasbaji et al., 2022)]:

$$log q_e = \frac{1}{n} \times \log C_e + \log K_F \quad (7)$$

where the Freundlich constants K_F (l/mg) and 1/n, which characterise the adsorption capacity and intensity, respectively, are used. The value of n, which ranges from 1 to 10, indicates how well the adsorption process works, and K_F, for the unit equilibrium concentration, is the amount of MB adsorbed on the adsorbent, 5% Mn_3O_4/Bi_2O_3. Moreover, the value of 1/n below one and closer to 0 indicates the more hetrogenisty of surface [(Bello et al., 2010; Ameta, 2020; Bindhu et al., 2021)]. In the present study, the value of 1/n is 0.3495 which suggests the adsorption of MB on the prepared adsorbent is a favorable and heterogeneous [(Ayawei et al., 2017)]. The adsorption parameters obtained in this study are presented in Table 4 whereas the representative plots (log C_e vs. log q_e) are shown in Figure.9B. Additionally, the low R^2 value (0.4444) for the Freundlich model in this study as compared to other isotherms indicates the absence of multilayer physisorption.

The Temkin model explains how the adsorbate and adsorbent interactions affect the adsorption mechanism. It implies that when

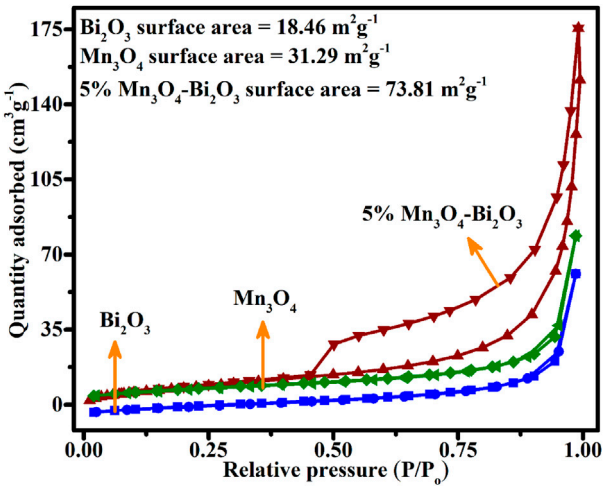

FIGURE 11
N_2 adsorption-desorption isotherms of Bi_2O_3, Mn_3O_4, and 5% Mn_3O_4-Bi_2O_3.

the number of adsorbate molecules increases on the adsorbent surface, the heat of adsorption (ΔH_{ads}) decreases. The Temkin isotherm is expressed according to the following equations [(Kasbaji et al., 2022)]:

$$q_e = BlnA_T + B\ln C_e \tag{8}$$

where,

$$B = \frac{RT}{b_T} \tag{9}$$

The Temkin constant for the heat of adsorption is b_T (J/mol), while the equilibrium binding constant is A_T (l/g). The values of the constants are calculated from the slope and intercept of the plot in Figure 9C, which is q_e vs. ln C_e. The obtained values of b_T and A_T are presented in Table 4 which are 2565 *J/mol* and 12.2 l/*g*, respectively with 0.8397 R^2 value in this investigation.

Dubinin-Raduskavich-Kaganer (DRK) is a semiempirical adsorption isotherm, which is primarily designed to express the Gaussian Energy distribution onto the heterogeneous surface of an adsorbent. It assumes that adsorption occurs through pore filling multilayer physical mechanism. DRK is a temperature-dependent model. The model is expressed by the following equation [(Kasbaji et al., 2022)]:

$$ln\, q_e = ln(q_d) - K_{DRK}\,\epsilon^2 \tag{10}$$

where ϵ is Polyani potential which is represented as [(Kasbaji et al., 2022)]:

$$\epsilon = RT\ln\left(\frac{1}{1+C_e}\right) \tag{11}$$

K_{DRK} (mol^2/kJ^2) is the Dubinin-Raduskavich-Kaganer constant which is relates to free adsorption energy, whereas q_d (*mg/g*) is the theoretical adsorption ability. The values of these constants K_{DRK} and q_d are mentioned in Table 4 which are 4×10^{-8} mol^2/kJ^2 and 0.5369 *mg/g*, respectively. These values are estimated by interpreting the slope and intercept of the plot presented in Figure 9D. It distinguishes between physical and chemical adsorption with its mean free adsorption energy, E calculated as [(Kasbaji et al., 2022)]:

$$E = -\left[\frac{1}{\sqrt{2K_{DRK}}}\right] \tag{12}$$

The value of *E* greater than 7 *kJ/mol* indicates the nature of chemical adsorption. The R^2 value for DRK model obtained from the plot in Figure 9D is 0.5282, which is not very ideal, and this shows the following mechanism does not follow the DRK model.

It is evident from the adsorption isotherms that the adsorption of MB on 5% Mn_3O_4-Bi_2O_3 follows the Langmuir isotherm the best. The decreasing trend of validity of adsorption isotherms based on R^2 value is; Langmuir isotherm > Temkin isotherm > Dubinin-Radushkevich isotherm > Freundlich isotherm.

The Langmuir model has a higher R^2 correlation coefficient than the other isotherms, at 0.9361. This validates the monolayer methylene blue adsorption on the surface of the 5 percent Mn_3O_4-Bi_2O_3 adsorbent. Additionally, it is stated that the value of "n" indicates if the adsorption process is appropriate; in this study, the value, 2.86, falls between 1 and 10 and favours the phenomena of sorption [(Bello et al., 2010; Ameta, 2020)]. The adsorption process uses chemisorption, and there are barely any interactions between the methylene blue molecules that have been adsorbed on the surface of the adsorbent. The adsorption technique was more advantageous since the separation factor's R_L value was less than 1.

The Temkin isotherm's R^2 value, which is 0.8397, indicates that the adsorption process somewhat resembles the Temkin model. From this information, it is inferred that the interaction between MB molecules and adsorbent increases due to the increase in surface coverage of 5% Mn_3O_4-Bi_2O_3 adsorbent. Moreover, the validity of Temkin model confirms the chemisorption process of MB onto 5% Mn_3O_4-Bi_2O_3 [(Ayawei et al., 2017)].

Recycling of 5% Mn_3O_4-Bi_2O_3 adsorbent

The 5% Mn_3O_4-Bi_2O_3 adsorbent was used in four cycles for the adsorption of 30 ppm MB and increase in concentration of unadsorbed MB dye was noticed as shown in the Figure 10. It is observed from the plot that ~95, ~90, ~83, and ~76% MB dye was removed by 5% Mn_3O_4-Bi_2O_3 in 1st, 2nd, 3rd, and 4th cycle, respectively. It is inferred from this recycling study that the adsorbent material can be successfully recycled and reused for the removal of MB even after four cycles.

BET analysis

The surface areas of Bi_2O_3, Mn_3O_4, and Mn_3O_4-Bi_2O_3 have been calculated using isotherms of nitrogen absorption and desorption. The observed isotherms correlate to mesoporous structures when compared to the Mn_3O_4-Bi_2O_3 composites isotherm pattern and the IUPAC standard isotherm pattern. The Mn_3O_4-Bi_2O_3 has a higher surface area of 73.81 m^2g^{-1} than that of Bi_2O_3 (18.46 m^2g^{-1}) and Mn_3O_4 (31.29 m^2g^{-1}), according to the N_2 adsorption-desorption isotherm findings (Figure 11). The potential for adsorption of nanocomposites with large surface areas is thought to be increased by the synergism effect of individual nanoparticles. The mesoporous Mn_3O_4-Bi_2O_3 composites, however, can successfully boost surface active sites, improving the adsorbent's adsorption properties.

Antifungal activity

Bi_2O_3, Mn_3O_4, and 5% Mn_3O_4-Bi_2O_3 were further tested for their antifungal effectiveness against *A. solani* and *M. fructicola* using the agar well-diffusion method and amphotericin B as a reference. With zone inhibition values of 58.6 and 53.9 mm, 5 percent 5% Mn_3O_4-Bi_2O_3display stronger antifungal capability than Bi_2O_3 and Mn_3O_4, according to the antifungal activity data (Table 5). The 5% Mn_3O_4-Bi_2O_3 composites interface with the fungal cell membrane, cling to functional protein groups, and ultimately cause fungal cell death due to their high surface area. The synergistic interaction of 5% Mn_3O_4-Bi_2O_3 composites and high surface area led to the increased antifungal impact.

Conclusion

Mn_3O_4-Bi_2O_3 adsorbents were successfully prepared through wet-impregnation method and smaller aggregates of Mn_3O_4 were noticed on monoclinic α-Bi_2O_3 surface. The composite nature of the adsorbent was verified through FTIR, XRD, SEM and XPS analyses. Among the prepared adsorbents, 5% Mn_3O_4-Bi_2O_3 was found efficient to remove 30 ppm MB at 28 ° C, 7 pH and 250 rpm shaking speed. In this study, contact time and dye concentration were found to be significant variables that affect the adsorption mechanism. It has been found that the adsorption capacity improves from 0.05 to 1.4 mg/g when the dye concentration is increased from 5 to 30 ppm. The adsorption process of MB onto 5% Mn_3O_4-Bi_2O_3 is inferred from the kinetic models and adsorption isotherms to have followed the pseudo 2nd order model and Langmuir isotherm, which indicate the chemisorption of MB by building monolayer on the adsorbent's surface. Through FTIR and TGA/DSC investigations, the adsorption of MB dye on 5% Mn_3O_4-Bi_2O_3 was also confirmed. These results support the notion that 5% Mn_3O_4-Bi_2O_3 can be employed as a reliable and recyclable adsorbent to remove the MB colour from contaminated water.

Data availability statement

The original contributions presented in the study are included in the article/supplementary material, further inquiries can be directed to the corresponding authors.

Author contributions

SIA: Conception, reviewed original manuscript and critical revision, acquisition of data and funding acquisition. AsA: She wrote the antifungal analysis part in the manuscript, interpreted the data and critical revision. MTQ: Conception, design of study, writing-original draft preparation. AhA: He wrote the UV-vis application part in the manuscript, interpreted the data and critical revision. SI: Interpret the data, performed major experimental works, writing-original draft preparation and editing. MTA: Performed UV-vis analysis, reviewed original manuscript and critical revision. MA: He wrote the BET analysis part in the manuscript, interpreted the data and critical revision. MAQ: Reviewed original manuscript, and critical revision. AB: He performed synthesis methodology. NSA: Visualization of data, XRD analysis, funding acquisition, writing reviewing, and editing. YJ: Conception, visualization of data, performed bandgap analysis, funding acquisition. EBE: Visualization of data, reviewed original manuscript and critical revision. All authors listed have made a substantial, direct, and intellectual contribution to the work and approved it for publication.

Funding

The author thankfully acknowledge the funding provided by Scientific Research Deanship, King Khalid University, Abaha, Kingdom of Saudi Arabia, under the grant number R.G.P.1/267/43. The researchers would like to acknowledge Deanship of Scientific Research, Taif University for funding this work. This research was funded by Princess Nourah bint Abdulrahman University Researchers Supporting Project number (PNURSP2023R58), Princess Nourah bint Abdulrahman University, Riyadh, Saudi Arabia. The authors thank Department of Chemistry, Forman Christian College (A Chartered University) Lahore Pakistan for supporting this work. The authors extend their appreciation to the Research Center at AlMaarefa University for funding this work.

Acknowledgments

The author thankfully acknowledge the funding provided by Scientific Research Deanship, King Khalid University, Abaha, Kingdom of Saudi Arabia, under the grant number R.G.P.1/267/43. The researchers would like to acknowledge Deanship of Scientific Research, Taif University for funding this work. This research was funded by Princess Nourah bint Abdulrahman University Researchers Supporting Project number (PNURSP2023R58), Princess Nourah bint Abdulrahman University, Riyadh, Saudi Arabia. The authors thank Department of Chemistry, Forman Christian College (A Chartered University) Lahore Pakistan for supporting this work. The authors extend their appreciation to the Research Center at AlMaarefa University for funding this work.

Conflict of interest

The authors declare that the research was conducted in the absence of any commercial or financial relationships that could be construed as a potential conflict of interest.

Publisher's note

All claims expressed in this article are solely those of the authors and do not necessarily represent those of their affiliated organizations, or those of the publisher, the editors and the reviewers. Any product that may be evaluated in this article, or claim that may be made by its manufacturer, is not guaranteed or endorsed by the publisher.

References

Abou-Gamra, Z. M., and Ahmed, M. A. (2015). TiO_2 nanoparticles for removal of malachite green dye from waste water. *Adv. Chem. Eng. Sci.* 5 (03), 373–388. doi:10.4236/aces.2015.53039

Adam, F. A., Ghoniem, M., Diawara, M., Rahali, S., Abdulkhair, B. Y., Elamin, M., et al. (2022). Enhanced adsorptive removal of indigo carmine dye by bismuth oxide doped MgO based adsorbents from aqueous solution: Equilibrium, kinetic and computational studies. *RSC Adv.* 12, 24786–24803. doi:10.1039/d2ra02636h

Ahmadi, S., Mohammadi, L., Rahdar, A., Rahdar, S., Dehghani, R., Adaobi Igwegbe, C., et al. (2020). Acid dye removal from aqueous solution by using neodymium (III) oxide nanoadsorbents. *Nanomaterials* 10, 556. doi:10.3390/nano10030556

Al-Ghouti, M. A., Khraisheh, M. A., Ahmad, M. N., and Allen, S. (2009). Adsorption behaviour of methylene blue onto Jordanian diatomite: A kinetic study. *J. Hazard. Mater.* 165 (1-3), 589–598. doi:10.1016/j.jhazmat.2008.10.018

Al-Gorair, A. S., Sayed, A., and Mahmoud, G. A. (2022). Engineered superabsorbent nanocomposite reinforced with cellulose nanocrystals for remediation of basic dyes: Isotherm, kinetic, and thermodynamic studies. *Polymers* 14 (3), 567. doi:10.3390/polym14030567

Alhogbi, B. G., Aslam, M., Hameed, A., and Qamar, M. T. (2020). The efficacy of Co_3O_4 loaded WO3 sheets for the enhanced photocatalytic removal of 2, 4, 6-trichlorophenol in natural sunlight exposure. *J. Hazard. Mater.* 397, 122835. doi:10.1016/j.jhazmat.2020.122835

Allen, S. J., and Koumanova, B. (2005). Decolourisation of water/wastewater using adsorption. *J. Univ. Chem. Technol. Metallurgy* 40 (3), 175–192.

Alomar, T. S., AlMasoud, N., Sharma, G., Alothman, Z. A., and Naushad, M. (2021). Incorporation of trimetallic nanoparticles to the SiO_2 matrix for the removal of methylene blue dye from aqueous medium. *J. Mol. Liq.* 336, 116274. doi:10.1016/j.molliq.2021.116274

Alshorifi, F. T., Ali, S. L., and Salama, R. S. (2022). Promotional synergistic effect of Cs–Au NPs on the performance of Cs–Au/$MgFe_2O_4$ catalysts in catalysis 3, 4-Dihydropyrimidin-2 (1H)-Ones and degradation of RhB Dye. *J. Inorg. Organomet. Polym. Mater.* 32 (10), 3765–3776. doi:10.1007/s10904-022-02389-8

Amadi, O., Odidiozor, C., and Okoro, I. (2017). Sorption kinetic and intraparticle diffusivities of As^{3+} and Hg^{2+} detoxification from aqueous solution using cellulosic biosorbent derived from okra (abelmoschus esculentus) stems. *Int. J. Eng. Inf. Syst.* 1 (8), 72–85.

Ameta, R. K. (2020). $[Fe(CN)_5NO]_2$--Based MOIFs for adsorption of organic pollutants and as a self-rotatory motor. *ACS omega* 6 (1), 456–464. doi:10.1021/acsomega.0c04896

Astuti, Y., Fauziyah, A., Nurhayati, S., Wulansari, A., Andianingrum, R., Hakim, A., et al. (2016). in Synthesis of α-Bismuth oxide using solution combustion method and its photocatalytic properties, *IOP Conference Series: Materials Science and Engineering* (Bristol, United Kingdom: IOP Publishing), 012006.

Ayawei, N., Ebelegi, A. N., and Wankasi, D. (2017). Modelling and interpretation of adsorption isotherms. *J. Chem.*, 2017, 1–11. doi:10.1155/2017/3039817

Ayub, A., Raza, Z. A., Majeed, M. I., Tariq, M. R., and Irfan, A. (2020). Development of sustainable magnetic chitosan biosorbent beads for kinetic remediation of arsenic contaminated water. *Int. J. Biol. Macromol.* 163, 603–617. doi:10.1016/j.ijbiomac.2020.06.287

Bakry, A. M., Alamier, W. M., Salama, R. S., El-Shall, M. S., and Awad, F. S. (2022). Remediation of water containing phosphate using ceria nanoparticles decorated partially reduced graphene oxide (CeO_2-PRGO) composite. *Surfaces Interfaces* 31, 102006. doi:10.1016/j.surfin.2022.102006

Basu, S., Ghosh, G., and Saha, S. (2018). Adsorption characteristics of phosphoric acid induced activation of bio-carbon: Equilibrium, kinetics, thermodynamics and batch adsorber design. *Process Saf. Environ. Prot.* 117, 125–142. doi:10.1016/j.psep.2018.04.015

Bello, O. S., Adelaide, O. M., Hammed, M. A., and Popoola, O. A. M. (2010). Kinetic and equilibrium studies of methylene blue removal from aqueous solution by adsorption on treated sawdust. *Macedonian J. Chem. Chem. Eng.* 29 (1), 77–85. doi:10.20450/mjcce.2010.181

Bindhu, B., Shaji, H., Kuruvila, K., Nazerine, M., and Shaji, S. (2021). in *Removal of total hardness using low cost adsorbents, IOP Conference Series: Materials Science and Engineering* (United States: IOP Publishing), 012089.

Birniwa, A. H., Mahmud, H. N. M. E., Abdullahi, S. S. a., Habibu, S., Jagaba, A. H., Ibrahim, M. N. M., et al. (2022). Adsorption behavior of methylene blue cationic dye in aqueous solution using polypyrrole-polyethylenimine nano-adsorbent. *Polymers* 14 (16), 3362. doi:10.3390/polym14163362

Dada, A. O., Latona, D. F., Ojediran, O. J., and Nath, O. O. (2016). Adsorption of Cu (II) onto bamboo supported manganese (BS-Mn) nanocomposite: Effect of operational parameters, kinetic, isotherms, and thermodynamic studies. *J. Appl. Sci. Environ. Manag.* 20 (2), 409–422. doi:10.4314/jasem.v20i2.24

Das, T. R., and Sharma, P. K. (2020). Bimetal oxide decorated graphene oxide (Gd_2O_3/Bi_2O_3@ GO) nanocomposite as an excellent adsorbent in the removal of methyl orange dye. *Mater. Sci. Semicond. Process.* 105, 104721. doi:10.1016/j.mssp.2019.104721

De Jesús Ruíz-Baltazar, Á., Reyes-López, S. Y., de Lourdes Mondragón-Sánchez, M., Robles-Cortés, A. I., and Pérez, R. (2019). Eco-friendly synthesis of Fe_3O_4 nanoparticles: Evaluation of their catalytic activity in methylene blue degradation by kinetic adsorption models. *Results Phys.* 12, 989–995. doi:10.1016/j.rinp.2018.12.037

El-Zahhar, A. A., and Awwad, N. S. (2016). Removal of malachite green dye from aqueous solutions using organically modified hydroxyapatite. *J. Environ. Chem. Eng.* 4 (1), 633–638. doi:10.1016/j.jece.2015.12.014

Faraji, M., Yamini, Y., and Rezaee, M. (2010). Magnetic nanoparticles: Synthesis, stabilization, functionalization, characterization, and applications. *J. Iran. Chem. Soc.* 7 (1), 1–37. doi:10.1007/bf03245856

Gómez-Pastora, J., Bringas, E., and Ortiz, I. (2014). Recent progress and future challenges on the use of high performance magnetic nano-adsorbents in environmental applications. *Chem. Eng. J.* 256, 187–204. doi:10.1016/j.cej.2014.06.119

Hameed, A., Aslam, M., Ismail, I. M., Salah, N., and Fornasiero, P. (2015). Sunlight induced formation of surface Bi_2O_4– x–Bi_2O_3 nanocomposite during the photocatalytic mineralization of 2-chloro and 2-nitrophenol. *Appl. Catal. B Environ.* 163, 444–451. doi:10.1016/j.apcatb.2014.08.029

Homaeigohar, S., Zillohu, A. U., Abdelaziz, R., Hedayati, M. K., and Elbahri, M. (2016). A novel nanohybrid nanofibrous adsorbent for water purification from dye pollutants. *Materials* 9 (10), 848. doi:10.3390/ma9100848

Hu, H., and Xu, K. (2020). "Physicochemical technologies for HRPs and risk control," in *High-risk pollutants in wastewater* (Amsterdam, Netherlands: Elsevier), 169–207.

Hu, X. S., Liang, R., and Sun, G. (2018). Super-adsorbent hydrogel for removal of methylene blue dye from aqueous solution. *J. Mater. Chem. A* 6 (36), 17612–17624. doi:10.1039/c8ta04722g

Ibrahim, A. A., Salama, R. S., El-Hakam, S. A., Khder, A. S., and Ahmed, A. I. (2021). Synthesis of 12-tungestophosphoric acid supported on Zr/MCM-41 composite with excellent heterogeneous catalyst and promising adsorbent of methylene blue. *Colloids Surfaces A Physicochem. Eng. Aspects* 631, 127753. doi:10.1016/j.colsurfa.2021.127753

Ishak, Z., and Kumar, D. (2022). Adsorption of methylene blue and reactive black 5 by activated carbon derived from tamarind seeds. *Trop. Aquatic Soil Pollut.* 2 (1), 1–12. doi:10.53623/tasp.v2i1.26

Kasbaji, M., Mennani, M., Grimi, N., Barba, F. J., Oubenali, M., Simirgiotis, M. J., et al. (2022). Implementation and physico-chemical characterization of new alkali-modified bio-sorbents for cadmium removal from industrial discharges: Adsorption isotherms and kinetic approaches. *Process Biochem.* 120, 213–226. doi:10.1016/j.procbio.2022.06.010

Khan, F., and Wahab, R. (2022). Utilization of solution grown manganese oxide nanocrystallite to microstructure against bacteria's inhibition. *J. Inorg. Organomet. Polym. Mater.* 32 (5), 1650–1667. doi:10.1007/s10904-021-02206-8

Krishnan, A., Ravindran, B., Balasubramanian, B., Swart, H. C., Panchu, S. J., and Prasad, R. (2022). *Emerging nanomaterials for advanced technologies*. Berlin, Germany: Springer.

Laurent, S., Forge, D., Port, M., Roch, A., Robic, C., Vander Elst, L., et al. (2008). Magnetic iron oxide nanoparticles: Synthesis, stabilization, vectorization, physicochemical characterizations, and biological applications. *Chem. Rev.* 108 (6), 2064–2110. doi:10.1021/cr068445e

Li, C., Liu, H., Jiang, X., Waterhouse, G. I., Zhang, Z., and Yu, L. (2018). Hierarchical Fe_3O_4/C with a flower-like morphology: A highly efficient and reusable dye adsorbent. *Synth. Met.* 246, 45–56. doi:10.1016/j.synthmet.2018.09.010

Li, H., Liu, L., Cui, J., Cui, J., Wang, F., and Zhang, F. (2020). High-efficiency adsorption and regeneration of methylene blue and aniline onto activated carbon from waste edible fungus residue and its possible mechanism. *RSC Adv.* 10 (24), 14262–14273. doi:10.1039/d0ra01245a

Li, L., Xiao, J., Liu, P., and Yang, G. (2015). Super adsorption capability from amorphousization of metal oxide nanoparticles for dye removal. *Sci. Rep.* 5, 9028–9036. doi:10.1038/srep09028

Li, N., Wang, J.-Y., Liu, Z.-Q., Guo, Y.-P., Wang, D.-Y., Su, Y.-Z., et al. (2014). One-dimensional ZnO/Mn 3 O 4 core/shell nanorod and nanotube arrays with high supercapacitive performance for electrochemical energy storage. *Rsc Adv.* 4 (33), 17274–17281. doi:10.1039/c4ra00588k

Li, Y., Lu, H., Wang, Y., Zhao, Y., and Li, X. (2019). Efficient removal of methyl blue from aqueous solution by using poly (4-vinylpyridine)–graphene oxide–Fe_3O_4 magnetic nanocomposites. *J. Mater. Sci.* 54, 7603–7616. doi:10.1007/s10853-019-03441-8

Mahmoud, M., and Mahmoud, A. S. (2021). Wastewater treatment using nano bimetallic iron/copper, adsorption isotherm, kinetic studies, and artificial intelligence neural networks. *Emergent Mater.* 4 (5), 1455–1463. doi:10.1007/s42247-021-00253-y

Mittal, H., Morajkar, P. P., Al Alili, A., and Alhassan, S. M. (2020). *In-situ* synthesis of ZnO nanoparticles using gum Arabic based hydrogels as a self-template for effective malachite green dye adsorption. *J. Polym. Environ.* 28 (6), 1637–1653. doi:10.1007/s10924-020-01713-y

Naeem, S., Baheti, V., Militky, J., Wiener, J., Behera, P., and Ashraf, A. (2016). Sorption properties of iron impregnated activated carbon web for removal of methylene blue from aqueous media. *Fibers Polym.* 17, 1245–1255. doi:10.1007/s12221-016-6423-x

Naseri, K., and Allahverdi, A. (2019). Methylene blue adsorption by TiO_2-based nano-adsorbents: Performance evaluation and kinetic study. *Res. Chem. Intermed.* 45, 4863–4883. doi:10.1007/s11164-019-03866-5

Nayl, A. A., Abd-Elhamid, A. I., Arafa, W. A., Ahmed, I. M., AbdEl-Rahman, A. M., Soliman, H., et al. (2023). A novel P@ SiO_2 nano-composite as effective adsorbent to remove methylene blue dye from aqueous media. *Materials* 16 (2), 514. doi:10.3390/ma16020514

Palansooriya, K. N., Yang, Y., Tsang, Y. F., Sarkar, B., Hou, D., Cao, X., et al. (2020). Occurrence of contaminants in drinking water sources and the potential of biochar for water quality improvement: A review. *Crit. Rev. Environ. Sci. Technol.* 50 (6), 549–611. doi:10.1080/10643389.2019.1629803

Qamar, M. T., Aslam, M., Rehan, Z., Soomro, M. T., Ahmad, I., Ishaq, M., et al. (2017). MoO_3 altered ZnO: A suitable choice for the photocatalytic removal of chloro-acetic acids in natural sunlight exposure. *Chem. Eng. J.* 330, 322–336. doi:10.1016/j.cej.2017.07.168

Qamar, M. T., Aslam, M., Rehan, Z., Soomro, M. T., Basahi, J. M., Ismail, I. M., et al. (2017). The influence of p-type Mn_3O_4 nanostructures on the photocatalytic activity of ZnO for the removal of bromo and chlorophenol in natural sunlight exposure. *Appl. Catal. B Environ.* 201, 105–118. doi:10.1016/j.apcatb.2016.08.004

Rahman, H. L., Erdem, H., Sahin, M., and Erdem, M. (2020). Iron-incorporated activated carbon synthesis from biomass mixture for enhanced arsenic adsorption. *Water, Air, & Soil Pollut.* 231 (1), 6–17. doi:10.1007/s11270-019-4378-4

Raiyaan, G., Khalith, S., and Sheriff, M. (2021). Bio-adsorption of methylene blue dye using chitosan-extracted from Fenneropenaeus indicus shrimp shell waste. Journal. *Aquac. Mar. Biol.* 10 (4), 146–150.

Ramutshatsha-Makhwedzha, D., Mavhungu, A., Moropeng, M. L., and Mbaya, R. (2022). Activated carbon derived from waste orange and lemon peels for the adsorption of methyl orange and methylene blue dyes from wastewater. *Heliyon* 8 (8), e09930. doi:10.1016/j.heliyon.2022.e09930

Rápó, E., and Tonk, S. (2021). Factors affecting synthetic dye adsorption; desorption studies: A review of results from the last five years (2017–2021). *Molecules* 26 (17), 5419. doi:10.3390/molecules26175419

Shi, H., Li, W., Zhong, L., and Xu, C. (2014). Methylene blue adsorption from aqueous solution by magnetic cellulose/graphene oxide composite: Equilibrium, kinetics, and thermodynamics. *Industrial Eng. Chem. Res.* 53 (3), 1108–1118. doi:10.1021/ie4027154

Sood, S., Umar, A., Mehta, S. K., and Kansal, S. K. (2015). α-Bi_2O_3 nanorods: An efficient sunlight active photocatalyst for degradation of Rhodamine B and 2, 4, 6-trichlorophenol. *Ceram. Int.* 41 (3), 3355–3364. doi:10.1016/j.ceramint.2014.10.038

Tan, I., Ahmad, A. L., and Hameed, B. H. (2008). Adsorption of basic dye using activated carbon prepared from oil palm shell: Batch and fixed bed studies. *Desalination* 225 (1-3), 13–28. doi:10.1016/j.desal.2007.07.005

Tejada-Tovar, C., Villabona-Ortíz, Á., and Gonzalez-Delgado, Á. D. (2021). Adsorption of azo-anionic dyes in a solution using modified coconut (Cocos nucifera) mesocarp: Kinetic and equilibrium study. *Water* 13 (10), 1382. doi:10.3390/w13101382

Yagub, M. T., Sen, T. K., Afroze, S., and Ang, H. M. (2014). Dye and its removal from aqueous solution by adsorption: A review. *Adv. colloid interface Sci.* 209, 172–184. doi:10.1016/j.cis.2014.04.002

Yang, L., Zhang, Y., Liu, X., Jiang, X., Zhang, Z., Zhang, T., et al. (2014). The investigation of synergistic and competitive interaction between dye Congo red and methyl blue on magnetic $MnFe_2O_4$. *Chem. Eng. J.* 246, 88–96. doi:10.1016/j.cej.2014.02.044

Zaharia, C., Suteu, D., Muresan, A., Muresan, R., and Popescu, A. (2009). Textile wastewater treatment by homogenous oxidation with hydrogen peroxide. *Environ. Eng. Manag. J.* 8 (6), 1359–1369. doi:10.30638/eemj.2009.199

Zulkifli, Z. A., Razak, K. A., and Rahman, W. N. W. A. (2018). The effect of reaction temperature on the particle size of bismuth oxide nanoparticles synthesized via hydrothermal method, *AIP conference proceedings*, AIP Publishing LLC: United States. 020007.